BIOCHEMISTRY
including biophysical chemistry & molecular biology

Article

pubs.acs.org/biochemistry

Variants of Phosphotriesterase for the Enhanced Detoxification of the Chemical Warfare Agent VR

Andrew N. Bigley,[†] Mark F. Mabanglo,[†] Steven P. Harvey,[‡] and Frank M. Raushel*[,†]

[†]Department of Chemistry, Texas A&M University, College Station, Texas 77843, United States

[‡]U.S. Army Edgewood Chemical Biological Center, 5183 Blackhawk Road, Aberdeen Proving Ground, Maryland 21010, United States

ABSTRACT: The V-type organophosphorus nerve agents are among the most hazardous compounds known. Previous efforts to evolve the bacterial enzyme phosphotriesterase (PTE) for the hydrolytic decontamination of VX resulted in the identification of the variant L7ep-3a, which has a k_{cat} value more than 2 orders of magnitude higher than that of wild-type PTE for the hydrolysis of VX. Because of the relatively small size of the *O*-ethyl, methylphosphonate center in VX, stereoselectivity is not a major concern. However, the Russian V-agent, VR, contains a larger *O*-isobutyl, methylphosphonate center, making stereoselectivity a significant issue since the S_P-enantiomer is expected to be significantly more toxic than the R_P-enantiomer. The three-dimensional structure of the L7ep-3a variant was determined to a resolution of 2.01 Å (PDB id: 4ZST). The active site of the L7ep-3a mutant has revealed a network of hydrogen bonding interactions between Asp-301, Tyr-257, Gln-254, and the hydroxide that bridges the two metal ions. A series of new analogues that mimic VX and VR has helped to identify critical structural features for the development of new enzyme variants that are further enhanced for the catalytic detoxification of VR and VX. The best of these mutants has been shown to have a reversed stereochemical preference for the hydrolysis of VR-chiral center analogues. This mutant hydrolyzes the two enantiomers of VR 160- and 600-fold faster than wild-type PTE hydrolyzes the S_P-enantiomer of VR.

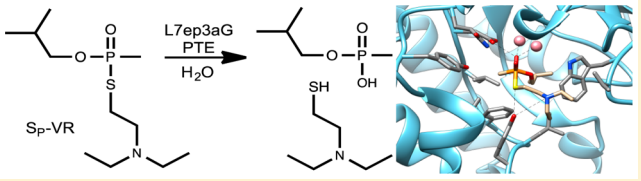

The organophosphorus nerve agents are among the most toxic compounds known. Compounds such as sarin, soman, and VX are all chiral methyl phosphonates where the toxicity of the S_P-enantiomer is much greater than that of the R_P-enantiomer.[1] Recent events have dramatically demonstrated the continuing importance of developing rapid and environmentally compatible methods for the decontamination of these compounds.[2] This situation is particularly true for the V-type nerve agents, where the lethal dose is approximately 6 mg/person, and these compounds have been shown to persist for long periods of time.[3,4] The current means of decontamination of chemical warfare agents relies on treatment with strong base, concentrated bleach, or high temperature incineration.

Medical intervention for nerve agent intoxication relies on compounds such as atropine, which reduces neurological symptoms, and oximes, which can help to reactivate the effected neural enzyme, acetylcholine esterase.[3] The only currently approved medical treatment for organophosphate poisoning, which acts directly on the nerve agent, is injection of the enzyme butyrylcholine esterase, which acts as a stoichiometric scavenger of organophosphonates.[5] The high specificity of enzyme catalyzed reactions also enables them to be exploited for analytical detection, as has been achieved using acetylcholine esterase in Disclosure Spray produced by FLIR Systems, which is used by the United States military.[6] Enzymatic means of environmental decontamination provide significant advantages over the harsher chemical or incendiary methods.

Several enzymes are known to hydrolyze organophosphate nerve agents, including human PON1, squid DFPase, and the bacterial enzymes OPAA and phosphotriesterase (PTE).[7−12] Among these enzymes, only PTE and PON1 are known to hydrolyze the V-type nerve agents. Wild-type PTE was used as the main ingredient in DEFENZ, which was marketed by Genencor for the decontamination of organophosphate nerve agents. Unfortunately, testing by the United States Environmental Protection Agency (EPA) found that while the enzyme formulation did hydrolyze a substantial portion of the nerve agents tested, the decontamination was not complete in the prescribed contact time.[13] PTE was successfully evolved for the decontamination of organophosphate insecticides and marketed as Landgauard A900 by CSIRO Ecosystem Sciences. While not currently licensed for sale in the United States, this product utilizes variants of PTE that have been evolved specifically to target organophosphorus insecticides.[14] At protein concentrations of 1 g/100 L of wastewater, 99% of the contaminants were neutralized within 12 h and the enzyme maintained >70% activity at room temperature for 6 months. PTE has also been formulated for application in firefighting foams, and shown to be effective for decontamination of paraoxon on surfaces and in soil.[15]

Significant advances have been made in developing specific PTE variants for the decontamination of G-type and VX nerve agents.[7,12] While wild-type PTE has reasonable activity against

Received: June 9, 2015
Revised: August 13, 2015
Published: August 14, 2015

ACS Publications © 2015 American Chemical Society

DOI: 10.1021/acs.biochem.5b00629
Biochemistry 2015, 54, 5502−5512

the G-type nerve agents ($k_{cat}/K_m \sim 10^5$ M^{-1} s^{-1}), this enzyme preferentially hydrolyzes the less toxic R_P-enantiomers.[16] Directed evolution of PTE to specifically target the G-type nerve agents has led to the identification of the variant H257Y/L303T (YT), which has proven highly efficient at the hydrolysis of the more toxic S_P-enantiomers of sarin (GB), soman (GD), and cyclosarin (GF) with values of k_{cat}/K_m that exceed 10^6 M^{-1} s^{-1}.[12]

Wild-type PTE exhibits little stereoselectivity against the relatively small phosphonate center of VX, but the elevated pK_a of the thiol-leaving group provides a significant challenge for enzyme-catalyzed hydrolysis ($k_{cat}/K_m \sim 10^2$ M^{-1} s^{-1}).[7] Mutation of residues contained within the active site of PTE resulted in the isolation of the variant H245Q/H257F (QF), which exhibited a 100-fold improvement for the hydrolysis of VX, relative to the wild-type enzyme (see Table 1 for identity of variants).[7]

Table 1. Identity of Parent Mutants of PTE

variant	mutations present
wild-type	none
QF	H254Q/H257F
CVQFL	I106C/F132V/H254Q/H257F/S308L
VRN-VQFL	A80V/F132V/K185R/H254Q/H257Y/I274N/S308L
L7ep-3a	I106C/F132V/H254Q/H257Y/A270V/L272M/I274N/S308L

Additional active site variations led to the identification of the mutant CVQFL (QF + I106C/F132V/S308L) with a similar catalytic efficiency for the hydrolysis of VX, but a 3-fold improvement in k_{cat}. The best variant identified to date for the hydrolysis of VX is VRN-VQFL (QF + F132V/S308L + A80V/K185R/I274N). This mutant combines expression-enhancing mutations (A80V/K185R/I274N) with additional changes in the active site to achieve a k_{cat}/K_m of 7×10^4 M^{-1} s^{-1} for the hydrolysis of the S_P-enantiomer of VX.[7,17,18] Expansion of the mutation strategy to targeted error-prone PCR led to the identification of the variant L7ep-3a (CVQFL + H257Y/A270V/L272M/I274N), which has a k_{cat} value enhanced 150-fold relative to wild-type PTE.[7] How these combined mutations, some of which do not fall in the active site, are able to bring about such a dramatic improvement in catalytic ability is not clear.

In addition to VX, the V-agents include the Russian (VR) and Chinese versions. Exemplified by VR, these additional V-agents contain a smaller thiol leaving group, and a larger ester group attached to the phosphorus center (Scheme 1). Wild-type PTE has enzymatic activity for the hydrolysis of racemic VR similar to VX, but the larger isobutyl group attached to the phosphorus center results in a 25-fold preference for the R_P-enantiomer.[16,19] The catalytic activity of wild-type PTE for the hydrolysis of the S_P-enantiomer of VR (k_{cat}/K_m = 4.3 M^{-1} s^{-1}) is significantly lower than for the hydrolysis of VX. PTE variants, which contain many of the same mutations as the VX-enhanced variants, have been reported to have substantially improved catalytic activity against S_P-VR.[20] Unfortunately, the in vivo toxicity of the individual enantiomers of VR has apparently not been reported. However, the S_P-enantiomer of VR has been shown to inactivate human acetylcholine esterase 2.2×10^4 times faster than does the R_P-enantiomer.[21] We have, therefore, made the explicit assumption that the S_P-enantiomer of VR is significantly more toxic than is the R_P-enantiomer, in accordance with the relative toxicities of the individual enantiomers of sarin, soman, and VX.[1]

Scheme 1

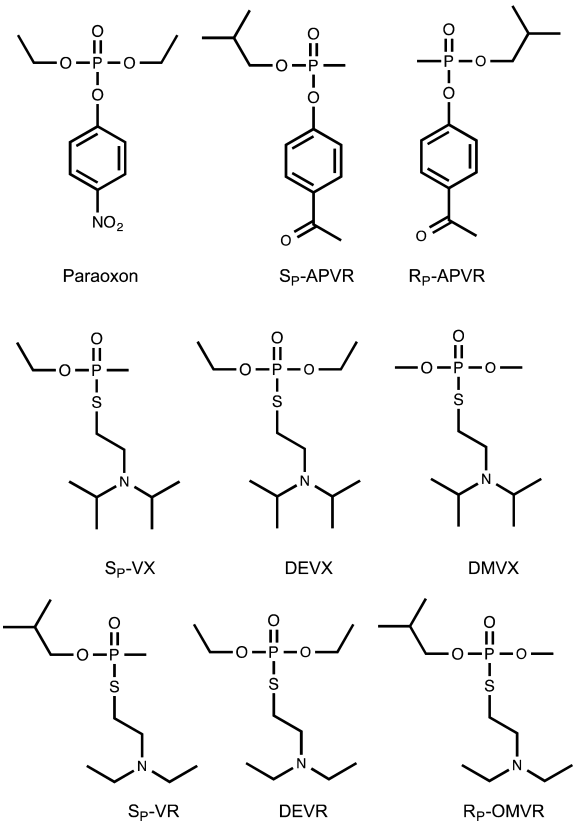

Currently, there is a lack of three-dimensional structural data that can be used to explain how the existing set of mutants are able to enhance the rate of hydrolysis of the phosphorothiolate bond in VX. In an effort to more completely understand the chemical mechanism for the enhancement of phosphorothiolate bond cleavage, the structure of the L7ep-3a variant was determined. With this new structural information, a series of PTE variants was created to incorporate changes in the active site of PTE that would more easily accommodate the *O*-isobutyl group of VR. To facilitate the further development of PTE for the hydrolysis of various V-agents, we have designed and synthesized a new series of analogues. Enhanced variants of PTE with improved activity toward the hydrolysis of the S_P-enantiomer of VR have been identified.

MATERIALS AND METHODS

Materials. Growth media and antibiotics were procured from Research Products Incorporated. DNA polymerase was obtained from Agilent. Other supplies for the molecular biology experiments were acquired from New England Biolabs. DEVX and *N*,*N*-diisopropylaminoethanethiol were synthesized as previously reported.[7,22] The individual enantiomers of *p*-acetophenyl VR (APVR) were synthesized as previously described.[16] Samples of VX and VR were Chemical Agent Standard Analytical Reference Material of the highest purity available, and were further purified as described previously.[7] Unless otherwise noted, all other chemicals were purchased from Sigma-Aldrich. The organophosphorus nerve agents used in this investigation are highly toxic and should be used with the proper safety precautions.

Synthesis of Dimethyl VX. Dimethyl VX (DMVX) was made by the reaction of dimethyl chlorophosphate with *N*,*N*-

DOI: 10.1021/acs.biochem.5b00629
Biochemistry 2015, 54, 5502−5512

diisopropylaminoethanethiol. *N*,*N*-Diisopropylaminoethanethiol (1.5 g; 9.3 mmol) was added to 100 mL of diethyl ether and allowed to cool in a dry ice/acetone bath before being purged with N_2. To this mixture was added 7.5 mL (2.0 equiv) of a 2.5 M solution of *n*-butyl lithium in hexanes and the reaction allowed to come to room temperature before recooling in a dry ice/acetone bath. Dimethyl chlorophosphate (2.0 g; 1.5 equiv) was mixed with 30 mL of diethyl ether in a separate flask and cooled. The dimethyl chlorophosphate solution was then added to the thiol solution and the reaction stirred at room temperature for 3 h. The reaction was brought to 400 mL with diethyl ether and extracted with water. The product was extracted into the aqueous phase with 0.5 M HCl. The aqueous phase was neutralized with sodium bicarbonate and extracted with dichloromethane. The organic phase was dried over Na_2SO_4, filtered, and evaporated to dryness. The product was further purified by silica gel chromatography. The product was dissolved in dichloromethane and eluted from the column using a 0−5% step gradient of methanol in dichloromethane. Fractions containing the desired product were combined and the solvent evaporated to provide the product as an oil. Overall isolated yield was 8%. ^{1}H NMR (300 MHz, $CDCl_3$): 3.84−3.77 (6H, d, J = 12.6 Hz, $OC\underline{H}_3$), 3.08−2.62 (6H, m, $SC\underline{H}_2C\underline{H}_2N(C\underline{H})_2$), 1.05−0.98 (12H, d, J = 6.9 Hz, $CH(C\underline{H}_3)_2$. ^{31}P NMR (121.4 MHz, $CDCl_3$): 32.74 ppm.

Synthesis of Diethyl VR. Diethyl VR (DEVR) was made by the reaction of diethyl chlorophosphate with *N*,*N*-diethylaminoethanethiol. *N*,*N*-Diethylaminoethanethiol was prepared from the hydrochloride salt by dissolving the compound in a saturated $NaHCO_3$ solution and extraction with diethyl ether. The organic phase was dried over Na_2SO_4 and evaporated in vacuo at room temperature. The remaining oil was distilled (50 °C) under high vacuum and recovered as a pure liquid in a dry ice cooled trap. *N*,*N*-Diethylaminoethanethiol (1.1 g; 8.35 mmol) was added to 100 mL of diethyl ether and cooled in a dry ice/acetone bath before being purged with N_2. To this mixture was added 10 mL (3.0 equiv) of a 2.5 M solution of *n*-butyl lithium in hexanes, and the reaction allowed to come to room temperature before recooling in a dry ice/acetone bath. Diethyl chlorophosphate (2.9 g; 2 equiv) was mixed with 30 mL of diethyl ether in a separate flask, purged with N_2, and then cooled in a dry ice/acetone bath. The cooled diethyl chlorophosphate solution was added to the thiol solution, and the reaction stirred at room temperature for 3 h. The reaction was brought to 400 mL with diethyl ether and extracted with water. The product was extracted into the aqueous phase with 0.5 M HCl. The aqueous phase was neutralized with sodium bicarbonate and extracted with dichloromethane. The organic phase was dried over Na_2SO_4, filtered, and then evaporated, yielding the product as an oil. Further purification was conducted using silica gel chromatography as described above. Overall yield of the isolated product was 7%. ^{1}H NMR (300 MHz, $CDCl_3$): 4.27−4.10 (4H, m, $OC\underline{H}_2CH_3$), 2.99−2.52 (8H, m, $SC\underline{H}_2C\underline{H}_2N(C\underline{H}_2)_2$), 1.43−1.34 (6H, t, J = 7.5 Hz, $OCH_2C\underline{H}_3$), 1.11−1.01 (6H, t, J = 7.2 Hz, $CH_2C\underline{H}_3$). ^{31}P NMR (121.4 MHz, $CDCl_3$): 28.50 ppm.

Synthesis of *O*-Methyl VR. *O*-Methyl VR (OMVR) was synthesized by the reaction of methyl isobutyl chlorophosphate with *N*,*N*-diethylaminoethanethiol. *N*,*N*-Diethylaminoethanethiol was prepared from the hydrochloride salt as described above. Methyl isobutyl chlorophosphate was prepared by dissolving 750 μL (8.4 mmol) of isobutanol in 50 mL of diethyl ether. The atmosphere was purged with N_2 and then the mixture was chilled in a dry ice/acetone bath. A total of 3.3 mL (1.0 equiv) of 2.5 M butyl lithium in hexanes and 1.5 g (1.0 equiv) of methyl dichlorophosphate was added, and the reaction stirred for 3 h at room temperature.

In a separate flask, 1.2 g (1.0 equiv) of *N*,*N*-diethylaminoethanethiol was dissolved in 50 mL of diethyl ether and chilled in a dry ice/acetone bath. A total of 5 mL (1.5 equiv) of 2.5 M *n*-butyl lithium was added and the reaction warmed to room temperature. The methyl isobutyl chlorophosphate and the thiol solutions were chilled in a dry ice/acetone bath and combined. The reaction was allowed to proceed at room temperature for 3 h. The reaction was then brought to 400 mL with diethyl ether and washed with water. The product was extracted with 0.5 M HCl, neutralized with sodium bicarbonate, and then extracted with dichloromethane. The organic phase was dried over Na_2SO_4 and evaporated to yield the product as an oil. Overall yield of final product was 15%. ^{1}H NMR (300 MHz, $CDCl_3$): 3.92−3.72 (5H, m, $OC\underline{H}_2CH(CH_3)_2$, $OC\underline{H}_3$), 2.95−2.45 (8H, m, $SC\underline{H}_2C\underline{H}_2N(C\underline{H}_2)_2$), 2.04−1.88 (1H, $OCH_2C\underline{H}(CH_3)_2$), 1.06−0.97 (6H, t, J = 7.0 Hz, $NCH_2C\underline{H}_3$), 0.97−0.90 (6H, d, J = 6.8 Hz, $OCH_2CH(C\underline{H}_3)_2$. ^{31}P NMR (121.4 MHz $CDCl_3$): 30.30 ppm.

Mutagenesis, Expression, and Enzyme Purification. The gene for PTE was cloned into the expression vector pET 20b between the NdeI and *Eco*RI restriction sites as previously described.[16] The new variants of PTE were generated by introducing the mutations Y309F, I106C, I106G, and L308S into the appropriate templates by site directed mutagenesis using the QuikChange (Agilent) protocol. DNA sequencing at the Gene Technologies Laboratory at Texas A&M University verified the specific mutations. The proteins were expressed and purified as previously described.[7] Briefly, the variants were freshly transformed into *E. coli* BL21 (DE3) cells by electroporation, and single colonies used to inoculate 5.0 mL cultures of LB medium. After 8 h of growth at 37 °C, 1.0 mL of this culture was used to inoculate 1 L cultures of Terrific Broth supplemented with 1.0 mM $CoCl_2$. The bacterial cultures were grown at 30 °C. IPTG was added to a final concentration of 1.0 mM after 24 h and growth continued for 40 h. The cells were harvested by centrifugation and stored at −80 °C prior to purification. Cells were resuspended in 100 mL of purification buffer (50 mM Hepes, pH 8.5, with 100 μM $CoCl_2$) and then lysed by sonication. The cell debris was cleared by centrifugation, and nucleic acids were precipitated by protamine sulfate (0.45 g in 20 mL purification buffer per liter of culture) and then removed by centrifugation. The PTE mutants were precipitated with ammonium sulfate (60% saturation) and recovered by centrifugation. The pellet was resuspended in ∼5 mL of purification buffer, filtered (0.45 μm), and loaded onto a GE Superdex 200 (16/60) preparatory size exclusion column using a BioRad NCG FPLC system. Fractions with catalytic activity for the hydrolysis of paraoxon were pooled and then eluted from a 3.0 g (dry weight) DEAE Sephadex A25 resin that was pre-equilibrated in purification buffer. Protein purity was verified by SDS-PAGE.

Enzymatic Activity. Catalytic activity with paraoxon was followed by monitoring the release of *p*-nitrophenol at 400 nm (ΔE_{400} = 17 000 M^{-1} cm^{-1}) in 250 μL reaction volumes containing 50 mM Ches, pH 9.0, 100 μM $CoCl_2$, and 0−1.0 mM paraoxon. Activity with APVR utilized the same reaction conditions as paraoxon with the release of the leaving group monitored at 294 nm (ΔE_{294} = 7710 M^{-1} cm^{-1}). Activity with DEVX, DMVX, DEVR, and OMVR was measured in 250 μL reactions containing 50 mM Hepes, pH 8.0, 100 μM $CoCl_2$, 0.3 mM DTNB, and 0−1.0 mM substrate. The release of the thiol leaving group was followed by inclusion of DTNB in the assay

DOI: 10.1021/acs.biochem.5b00629
Biochemistry 2015, 54, 5502−5512

Table 2. X-ray Crystallography Data for L7ep-3a and L7ep-3a I106G

variant (PDB)	L7ep-3a (4ZST)	L7ep-3a I106G (4ZSU)
resolution, Å (highest resolution shell)	50.00−2.01 (2.04−2.01)	50.00−2.01 (2.04−2.01)
space group	$P2_1$	$P2_1$
cell dimensions		
a	45.53	45.85
b	80.64	80.63
c	78.73	78.84
γ	106.60	106.94
R_{sym}	0.087	0.057
$I/\sigma I$	13.2 (3.0)	18.9 (2.8)
completeness, % (highest resolution shell)	98.3 (96.1)	95.8 (91.1)
redundancy (highest resolution shell)	3.5 (3.2)	3.7 (3.2)
refinement		
resolution, Å	29.61−2.01	29.57−2.01
no. of reflections	35 603	34 657
R_{work}/R_{free}	0.1574/0.2145	0.1348/0.1838
no. of nonhydrogen atoms		
total	5420	5395
water	383	384
B-factors		
protein	27.56	28.08
Co^{2+}	30.72	30.60
root mean square deviations		
bond lengths, Å	0.006	0.007
bond angles, deg	1.09	1.10
Ramachandran		
favored, %	97.4	97.1
allowed, %	2.6	2.9
outliers, %	0	0

mixture (ΔE_{412} = 14 150 M^{-1} cm^{-1}). All assays were initiated by the addition of the appropriately diluted enzyme and monitored in a 96-well format using a Molecular Devices SpectraMax 364 Plus plate reader. Reactions were monitored for 15 min at 30 °C and the linear portion of the time course was used to calculate the initial rate. Kinetic constants were determined by fitting the data to the Michaelis−Menten equation.[23] When saturation could not be observed, the data were fit to a linear equation and the slope taken as k_{cat}/K_m.

Stereoselective Hydrolysis of Racemic VX and VR. Low initial concentrations (19−160 μM) of racemic VX and VR were hydrolyzed by variants of PTE in a solution containing 0.1 mM $CoCl_2$, 0.3 mM DTNB, and 50 mM Bis-Tris-propane, pH 8.0. The reactions were followed to completion and the fraction hydrolyzed plotted as a function of time. The time courses were fit to eqs 1 and 2 where *F* is the fraction hydrolyzed, *a* and *b* are the magnitudes of the exponential phases, *t* is time, and k_1 and k_2 are the rate constants for each phase.[16]

$$F = a(1 - e^{-k_1 t}) \quad (1)$$

$$F = a(1 - e^{-k_1 t}) + b(1 - e^{-k_2 t}) \quad (2)$$

Stereochemical preferences were determined using the previously described complementation method.[7] Briefly, variants with large stereoselective preferences were placed in a reaction with mutants of PTE of known stereoselective preferences under conditions where each variant alone would exhibit a similar rate for the first exponential phase. If the variants prefer the same enantiomer, the resulting time course will exhibit two distinct phases. If the variants have the opposite enantiomers as the preferential substrate, the time courses will exhibit a single exponential phase.

pH−Rate Profiles. The pH−rate profiles for wild-type, QF, and L7ep-3a were determined using 100 μM paraoxon as the substrate in a combination buffer system using Mes, Mops, Hepes, and Ches buffers at 20 mM each. The pH of each stock buffer was adjusted to desired value using KOH, and the pH was verified after reactions to ensure no substantial change in pH had occurred. Reactions were carried out in 250 μL volumes using 96-well plates and followed at the pH-independent wavelength of 347 nm (ΔE_{347} = 5176 M^{-1} s^{-1}) as previously described.[24] Data were fit to eq 3 for the ionization of a single proton or eq 4 for two protons, where *y* is the enzymatic rate (s^{-1}) and *c* is the pH-independent value.

$$\log y = \log\left[\frac{c}{1 + 10^{(pK_a - pH)}}\right] \quad (3)$$

$$\log y = \log\left[\frac{c}{1 + 10^{(pK_a - pH)^2}}\right] \quad (4)$$

X-ray Crystallography. The PTE mutants L7ep-3a and L7ep-3a I106G were crystallized at 18 °C using the vapor diffusion method. In the crystallization experiments, 1.0 μL of protein (10 mg/mL with 1.0 mM $CoCl_2$) was mixed with 1.0 μL of the precipitant solution (100 mM sodium cacodylate pH 5.5−7.0, 0.2 M magnesium acetate, 15−30% PEG 8000), and then equilibrated against 500 μL of the same precipitant solution using Intelliplates. Protein crystals appeared within a week and grew to maximum dimensions (200 μm × 15 μm × 15 μm) after 21 days. Prior to data collection, the crystals were soaked for 30 s in a

DOI: 10.1021/acs.biochem.5b00629
Biochemistry 2015, 54, 5502−5512

cryoprotectant solution of the mother liquor containing 30% ethylene glycol and then frozen in liquid nitrogen. Diffraction data were collected at 120 K on an R-AXIS IV detector with Cu Kα X-rays produced from a rotating anode generator. X-ray data reduction and scaling were performed with HKL2000 (25).[25] Structures of the PTE mutants L7ep-3a and L7ep-3aG were determined by molecular replacement using the coordinates of wild-type PTE (PDB id: 1DPM) as the search model. The structures were built using COOT and refined with simulated annealing, B-factor randomization, and coordinate shaking using PHENIX.[26,27] Later stages of refinement were also done in PHENIX using individual coordinate, anisotropic B-factor, and occupancy optimization. The PTE mutant structures were refined with R_{work}/R_{free} values of 13.5−21.5% with excellent geometry (Table 2).

Computational Docking of High Energy Intermediates. The pentavalent high-energy reaction intermediate states for the hydrolysis of VX and VR were computationally docked into the three-dimensional structures of wild-type PTE (PDB id: 1DPM), H254Q/H257F (PDB id: 2OQL), L7ep-3a (PDB id: 4ZST), and L7ep-3aG (PDB id: 4ZSU). The high energy intermediate states for the hydrolysis of the R_P- and S_P-enantiomers were manually generated as trigonal bipyrimidal structures with the attacking hydroxyl group protonated and the original phosphoryl oxygen substituent carrying a full negative charge using ChemBio Ultra 14.0. Computational docking was done using the program AutoDock Vina.[28] The appropriateness of the docked poses was evaluated by the value of the distance of the attacking hydroxyl group from the α- and β-metal ions, the distance of the phosphoryl oxygen from the β-metal and the orientation of the side ester substituents into the large and small group pockets contained in the active site of PTE.

RESULTS

Three-Dimensional Structure of L7ep-3a. The PTE variant L7ep-3a has the highest reported k_{cat} for the hydrolysis of the nerve agent VX.[7] In an effort to elucidate the mechanism by which the activity of this mutant is enhanced, the enzyme was crystallized and the structure determined to a resolution of 2.01 Å by X-ray diffraction methods (PDB id: 4ZST). The overall structure of L7ep-3a is very similar to wild-type PTE (Figure 1A). The core of the $(\beta/\alpha)_8$-barrel matches very well between the two structures with a Cα RMSD of 0.64 Å. The only significant change in the backbone structure is apparent in the conformations of Loop-7 and Loop-8. In this variant, Loop-7, including the Loop-7 α-helix, is pulled toward the active site (Figure 1B). A portion of Loop-8 is similarly pulled toward the active site. Loop-8 also participates in the dimer interface, but the cross-interface interactions are all retained in the L7ep-3a mutant.

The binding site for the substrate in wild-type PTE is divided into the large-group pocket (His-254, His-257, Leu-271, and Met-317), the leaving-group pocket (Trp-131, Phe-132, Phe-306, and Tyr-309), and the small-group pocket (Gly-60, Ile-106, Lue-303, and Ser-308).[29] The mutations H257Y and S308L, coupled with the shifting of the Loop-7 α-helix, have induced significant changes in the substrate binding pockets in the active site of L7ep-3a. The side-chain of Tyr-309 is repositioned so that the phenolic group now extends into the active site rather than toward Loop-7, as previously observed in the structure of wild-type PTE (Figures 1B and 2). The reorientation of Tyr-309, along with the substitution of a tyrosine for His-257 and the repositioning of Leu-271 into the active site, has compressed the size of the large-group and leaving-group pockets. The leaving-group pocket is also constricted by the presence of the S308L mutation, which adds bulk to both the leaving-group and small-group pockets. However, the apparent contraction of the leaving-group pocket is partially relieved by the F132V mutation. Similarly, the I106C mutation opens additional space to the small-group pocket.

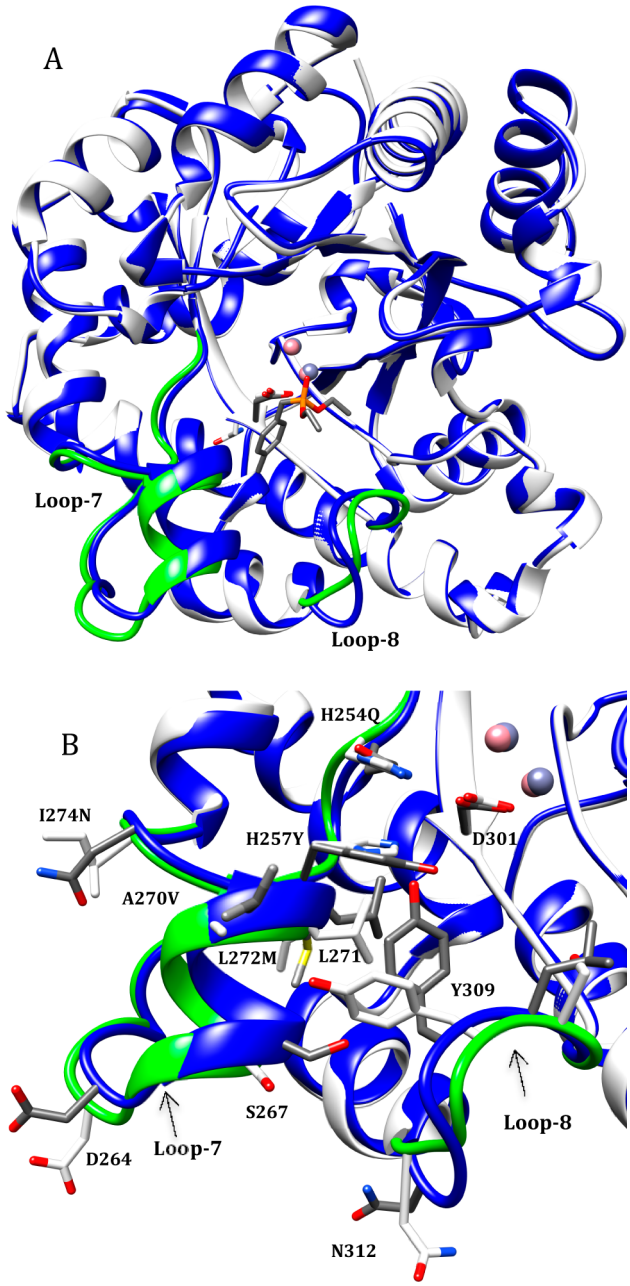

Figure 1. (A) Structural alignment between wild-type PTE (white) and L7ep-3a (blue). Selective active site residues are labeled and shown. Loop-7 and Loop-8 are colored green in the wild-type structure. (B) Expanded view of Loop-7 and Loop-8. Mutated residues and residues with significant structural perturbations are shown as sticks. The wild-type structure is taken from PDB id 1DPM, and the L7ep-3a structure is taken from PDB id 4ZST.

Generation and Characterization of New PTE Variants. The PTE variants QF, CVQFL, VRN-VQFL, and L7ep-3a were previously shown as having substantially improved activity for the hydrolysis of VX.[7] The stereoselectivity of these mutants for

DOI: 10.1021/acs.biochem.5b00629
Biochemistry 2015, 54, 5502−5512

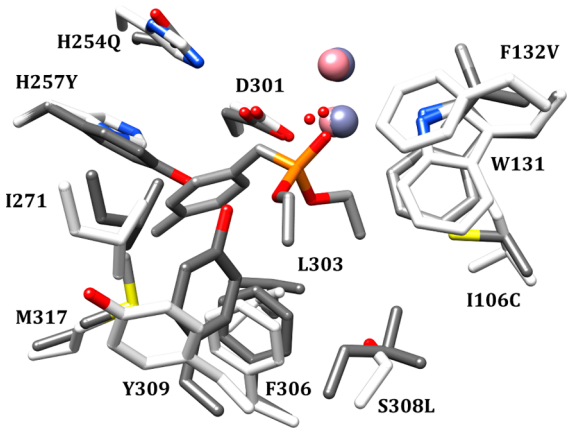

Figure 2. Substrate binding pockets of wild-type (white) and L7ep-3a (gray). The large-group pocket residues are His-254, His-257, Ile-271, and Met-317. The small-group pocket residues are Gly-60, Ile-106, Leu-303, and Ser-308. The leaving group pocket resides are Trp-131, Phe-132, Phe-306 and Tyr-309. The wild-type structure (PDB id: 1DPM) is shown with the inhibitor, diethyl 4-methylbenzylphosphonate, bound in the active site.

the chiral center contained in VR was determined using the isolated enantiomers of APVR (Table 3). With the exception of QF, the VX-optimized variants of PTE prefer to hydrolyze the R_P-enantiomer of the chiral center for VR. The crystal structure of L7ep-3a suggests that the mutations I106C and S308L alter the size of the small-group pocket. In order for the S_P-enantiomer of VR to productively bind in the active site, the larger isobutyl group must be positioned in the small-group pocket of PTE. In an effort to maximize the hydrolysis of S_P-VR, a series of new mutants was created from the original CVQFL and VRN-VQFL variants with residue 106 mutated to isoleucine, cysteine, or glycine in combination with residue position 308 being mutated to either leucine or serine. In an attempt to achieve the high k_{cat} seen previously for the hydrolysis of VX, the I106G variant of L7ep-3a was also constructed. The catalytic activities of these variants were first characterized against the insecticide paraoxon and the V-agent analogue DEVX (Table 4), and then the stereochemical preferences were determined using APVR (Table 3).

Isoleucine at residue position 106 favors hydrolysis of the R_P-enantiomer, while cysteine at position 106 reduces the preference for the R_P-enantiomer, and glycine leads to a preference for the S_P-enatiomer. For example, the CVQFL variant has a 2.5-fold preference for the R_P-enantiomer of the VR chiral center, but CVQFL-C106I has a 35-fold preference for the R_P-enantiomer. Despite this large difference in stereoselectivity, both of these variants hydrolyze DEVX with a k_{cat}/K_m of ~2 × 10^4 M^{-1} s^{-1}. When glycine was substituted at position 106, the stereochemical preference shifted to the S_P-enantiomer of APVR. L7ep-3a prefers the R_P-enantiomer by 1.5-fold, but L7ep-3a I106G prefers the S_P-enantiomer by 6.5-fold. Unfortunately, the I106G mutation reduced the activity against DEVX by more than an order of magnitude in these variants.

Serine at position 308 results in a much reduced stereoselectivity compared to leucine at position 308, but at the cost of catalytic efficiency with DEVX. VRN-VQFL prefers the R_P-enantiomer of APVR by 20-fold. The variant VRN-VQFL L308S has a preference of 1.2-fold, but the activity against DEVX was diminished 2-fold. Similarly, CVQFL prefers the R_P-enantiomer of APVR by 2.5-fold, while CVQFL-L308S prefers the R_P-enantiomer by 1.4-fold, but the catalytic activity is reduced ~5-fold for DEVX. The combination of glycine at residue position 106 with serine at 308 gave the best preference for the S_P-enantiomer of APVR, but also shows the biggest reduction in catalytic activity for DEVX. VRN-VQFL-I106G/L308S prefers the S_P-enantiomer by 14-fold, but activity with DEVX is reduced nearly 2-orders of magnitude to a third of that seen with the wild-type enzyme.

Catalytic Activity with VX and VR. The most promising new variants were tested at the Edgewood Chemical Biological Center with racemic VX and VR. The assays were conducted as the complete hydrolysis of a single low concentration of these agents to enable the observation of exponential time courses, corresponding to the hydrolysis of each enantiomer contained within the racemic mixture. The kinetic constants are presented

Table 3. Kinetic Constants for PTE Variants with APVR[a]

	R_P-APVR			S_P-APVR			
enzyme	k_{cat} (s^{-1})	K_m (mM)	k_{cat}/K_m (M^{-1} s^{-1})	k_{cat} (s^{-1})	K_m (mM)	k_{cat}/K_m (M^{-1} s^{-1})	ratio[c]
wild-type	84	1.7	4.9×10^4	25	4.5	6×10^3	8:1 *R*
QF	57	0.36	1.6×10^5	8.7	0.030	2.9×10^5	1.8:1 *S*
CVQFL	46	0.18	2.6×10^5	21	0.19	1.1×10^5	2.5:1 *R*
CVQFL C106I[b]	50	0.15	3.3×10^5	14	1.5	9.5×10^3	35:1 *R*
CVQFL-I106G	174	1.4	1.2×10^5	36	0.20	1.8×10^5	1.5:1 *S*
CVQFL-L308S[b]	122	2.0	6.0×10^4	8.1	0.19	4.2×10^4	1.4:1 *R*
CVQFL-I106G/L308S	100	4	2.4×10^4	40	0.24	1.6×10^5	6.7:1 *S*
VRN-VQFL	55	0.16	3.4×10^5	29	1.7	1.7×10^4	20:1 *R*
VRN-VQFL-I106C	72	0.23	3.2×10^5	33	0.23	1.4×10^5	2.3:1 *R*
VRN-VQFL-I106G	56	0.41	1.4×10^5	159	0.18	9.0×10^5	6.6:1 *S*
VRN-VQFL-L308S	17	0.52	3.2×10^4	5.0	0.13	3.9×10^4	1.2:1 *S*
VRN-VQF-I106C/L308S	160	1.7	1.0×10^5	51	1.5	3.4×10^4	3:1 *R*
VRN-VQFL-I106G/L308S	45	2.1	2.2×10^4	53	0.18	3.0×10^5	14:1 *S*
L7ep-3a	101	0.62	1.6×10^5	56	0.5	1.1×10^5	1.5:1 *R*
L7ep-3a I106G	58	0.71	8.2×10^4	166	0.31	5.3×10^5	6.5:1 *S*

[a]Errors from curve fitting are less than 10% with the exception of CVQFL-I106G/L308S, which has an error of 20% due to the high K_m value. [b]The mutations C106I and L308S are revertants back to the wild-type amino acid sequence. [c]The ratio is k_{cat}/K_m values for fast enantiomer and slow enantiomer, with the preferred enantiomer identified.

DOI: 10.1021/acs.biochem.5b00629
Biochemistry 2015, 54, 5502−5512

Table 4. Kinetic Parameters for PTE Variants with Paraoxon and DEVX[a]

enzyme	paraoxon			DEVX			fold improved[c]
	k_{cat} (s^{-1})	K_m (uM)	k_{cat}/K_m (M^{-1} s^{-1})	k_{cat} (s^{-1})	K_m (mM)	k_{cat}/K_m (M^{-1} s^{-1})	
wild-type	2230	81	2.8×10^7	1.1	0.87	1.2×10^3	
QF	41	5.3	7.7×10^6	6.1	1.4	4.2×10^3	3.5
CVQFL	38	5.6	6.8×10^6	16	0.76	2.1×10^4	17
CVQFL-C106I[b]	66	5.4	1.2×10^7	14	0.65	2.2×10^4	18
CVQFL-L308S[b]	33	6.7	4.8×10^6	13	3.2	4.1×10^3	3.4
CVQF-I106G/L308S	48	25	1.9×10^6	nd	nd	3.1×10^2	0.3
CVQFL-C106I/L308S	108	11	1.0×10^7	19	1.0	1.9×10^4	16
CVQFL-I106G	456	22	2.0×10^7	31	2.8	1.1×10^4	9.2
VRN-VQFL	116	8	1.5×10^7	22	0.73	3.1×10^4	26
VRN-VQFL-I106C	103	5.3	1.9×10^7	23	0.80	2.8×10^4	23
VRN-VQFL-I106G	446	21	2.1×10^7	nd	nd	5.0×10^3	4.2
VRN-VQFL-L308S	15	1.7	8.8×10^6	5.1	0.35	1.5×10^4	13
VRN-VQFL-I106C/L308S	35	3.6	9.7×10^6	8.6	1.6	5.4×10^3	4.5
VRN-VQFL-I106G/L308S	58	9.2	6.2×10^6	nd	nd	4.1×10^2	0.3
L7ep-3a	85	7.2	1.2×10^7	51	0.60	8.5×10^4	71
L7ep-3a I106G	545	33	1.67×10^7	nd	nd	7.7×10^3	6.4
L7ep-3a Y309F	131	9.2	1.43×10^7	36	1.2	3.0×10^4	25

[a]Errors from curve fitting were less than 10%. [b]The mutations C106I and L308S are revertants to the wild-type amino acid sequence. [c]k_{cat}/K_M of variant divided by k_{cat}/K_m of wild-type.

Table 5. Kinetic Constants with the Racemic Nerve Agents VX and VR[a]

enzyme	VX			VR			fold improved[d]
	k_{cat}/K_{m1} (M^{-1} s^{-1})	k_{cat}/K_{m2} (M^{-1} s^{-1})	ratio	k_{cat}/K_{m1} (M^{-1} s^{-1})	k_{cat}/K_{m2} (M^{-1} s^{-1})	ratio[c]	
wild-type	8.4×10^1	nd		1.1×10^2	4.3×10^0	25:1 *R*	
QF	1.7×10^4	1.5×10^3	12:1 *S*	4.8×10^2	7.9×10^1	6:1	4.4
CVQFL	1.0×10^5		1:1	5.5×10^3	8.9×10^2	6:1	50
VRN-VQFL	1.1×10^5	4.3×10^4	4:1	2.4×10^3	nd	>30:1 *R*	22
VRN-VQFL-I106G	6.6×10^3		1:1	2.0×10^3	4.1×10^2	5:1	18
VRN-VQFL-L308S[b]	6.2×10^4	8.9×10^3	7:1	2.7×10^2		1:1	2.5
VRN-VQFL-I106G/L308S	4.9×10^3	1.7×10^3	3:1	2.1×10^3	6.7×10^1	31:1 *S*	19
L7ep-3a	8.3×10^5	2.2×10^5	4:1	2.2×10^3	2.1×10^2	10:1	20
L7ep-3a I106G	2.0×10^4	6.2×10^3	3:1	2.6×10^3	6.9×10^2	3.8:1	56

[a]Errors from curve fitting are less than 5%. [b]The mutation L308S is a revertant to the wild type amino acid sequence. [c]The ratio is k_{cat}/K_m values for fast enantiomer and slow enantiomer. If the preferred enantiomer is not listed it has not been determined. [d]k_{cat}/K_{m1} of variant divided by k_{cat}/K_{m1} of wild-type.

in Table 5. For enzyme variants with large stereochemical preferences, the identity of the preferred enantiomer was determined by the ability of the variant to complement the slow phase of a variant of known preference. Wild-type PTE is known to prefer to hydrolyze the R_p-enantiomer of the VR chiral center, while QF is known to prefer the S_p-enantiomer of VX.[7,16] None of the variants tested, with the exception of QF, exhibited large stereochemical preferences for hydrolysis of the two enantiomers of VX. Removal of the S308L mutation (VRN-VQFL L308S) resulted in a 2-fold reduction in catalytic activity for the faster enantiomer of VX and a 5-fold reduction in the rate of hydrolysis for the slower enantiomer. Introduction of the I106G mutation (VRN-VQFL-I106G) led to the complete hydrolysis of racemic VX without detectable selectivity, but at a rate 6-fold slower than VRN-VQFL had for the slower enantiomer.

With racemic VR, the VRN-VQFL variant exhibited a 20-fold enhancement in the rate of hydrolysis compared to the wild-type enzyme, but this mutant was found to only hydrolyze the less toxic R_p-enantiomer of VR. Removal of the S308L mutation (VRN-VQFL L308S) enabled the hydrolysis of both enantiomers of VR, with complete loss of stereoselectivity. This represents a 64-fold improvement toward the hydrolysis of the toxic S_p-enantiomer compared to wild-type PTE. The introduction of the I106G mutation in the VRN-VQFL-I106G/L308S variant resulted in a strong preference for the hydrolysis of the S_p-enantiomer relative to the R_p-enantiomer. VRN-VQFL-I106G, which has both the I106G and S308L mutations, has much less stereochemical preference, but the kinetic data for the hydrolysis of the two enantiomers of APVR indicate that the stereochemical preference is for the S_p-enantiomer. The best variant identified for the hydrolysis of VR was L7ep-3a I106G, which has a k_{cat}/K_m of 2.6×10^3 M^{-1} s^{-1} for the faster enantiomer. While the stereoselectivity was not sufficient to determine the stereochemical preference with VR directly, the kinetic data with the two enantiomers of APVR has identified the preferred enantiomer as the S_p-enatiomer. The L7ep-3a I106G mutant thus has a 620-fold enhanced rate of hydrolysis of S_p-VR relative to wild-type PTE.

Three-Dimensional Structure of L7ep-3a I106G. In an effort to understand the physical basis for the observed improvement in the catalytic activity of L7ep-3a I106G, the three-dimensional structure was solved by X-ray crystallography (PDB id: 4ZSU). The core structure is very similar to wild-type

DOI: 10.1021/acs.biochem.5b00629
Biochemistry 2015, 54, 5502−5512

PTE (Cα RMSD = 0.66 Å) and the loop structure matches that observed with L7ep-3a.

pH−Rate Profiles for PTE. The pH−rate profiles for wild-type PTE, QF, and L7ep-3a with cobalt as the active site metal were determined with paraoxon as the substrate (Figure 3). The

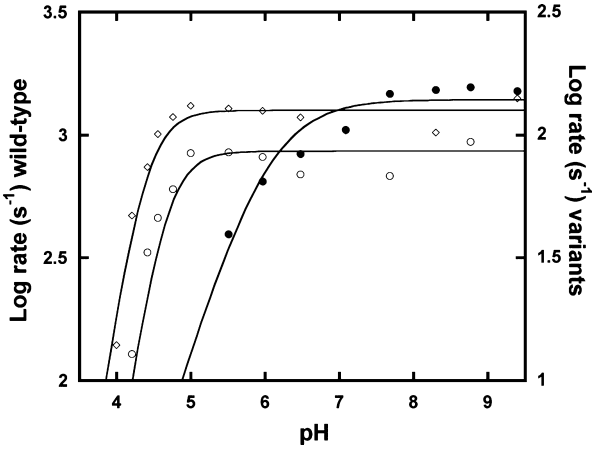

Figure 3. pH−rate profiles for wild-type PTE (●), L7ep-3a (○), and QF (◇).

wild-type enzyme exhibits the loss of activity by the protonation of a single group with an observed pK_a of 5.9. The QF and L7ep-3a variants have pK_a values of 4.4 and 4.6, respectively. For both of these variants the pH rate profiles indicate that two groups are protonated at low pH.

Evaluation of New V-Agent Analogues. The majority of research targeting the catalytic hydrolysis of organophosphorus nerve agents must be done using analogues for both regulatory and safety reasons. Intrinsic to the use of substrate analogues is the imperfect representation of catalytic activity with the authentic nerve agent. To address which structural factors of the VR and VX analogues are most significant, the compounds DMVX, DEVR, and OMVR were synthesized and analyzed as substrates for the optimized mutants of PTE and compared with the ability of these mutants to hydrolyze the S_P-enantiomers of VR and VX. The catalytic activity using these compounds was determined with a series of variants for which the hydrolysis of authentic nerve agents was available (Table 6). Wild-type PTE has a much lower catalytic activity with DMVX (k_{cat}/K_m = 1.9 × 10^1 M^{-1} s^{-1}) than was observed with DEVX (k_{cat}/K_m 1.2 × 10^3 M^{-1} s^{-1}). The best variant with DMVX was L7ep-3a, which has a k_{cat} = 28 s^{-1} and a k_{cat}/K_m = 1.3 × 10^4 M^{-1} s^{-1}. These values are 1,300- and 680-fold better, respectively, than wild-type PTE. Compared to DMVR, wild-type PTE exhibits better catalytic activity with DEVR (k_{cat}/K_m = 5.6 × 10^2 M^{-1} s^{-1}), but L7ep-3a also had the best catalytic activity with this analogue (k_{cat}/K_m = 1.5 × 10^4 M^{-1} s^{-1}). With the exception of wild-type PTE (k_{cat}/K_m = 6.8 × 10^1 M^{-1} s^{-1}), racemic OMVR gave the least activity for most of the variants tested. The combination of poor solubility of this compound and high K_m values limited analysis to the determination of k_{cat}/K_m for most variants. The best mutant for the hydrolysis of OMVR was L7ep-3a with a k_{cat}/K_m = 5.8 × 10^2 M^{-1} s^{-1}. However, given the switch in stereochemical preference, it is highly likely that L7ep-3a I106G has the best catalytic activity with the R_P-enantiomer of OMVR (which corresponds to the same relative stereochemistry as the S_P-enantiomer of VR).

DISCUSSION

Comparison of Substrate Analogues. The VX analogue DEVX was successfully used to identify PTE variants for the hydrolysis of VX, but it overestimated the activity of the wild-type enzyme and failed to detect a 100-fold increase in the catalytic activity with the QF variant.[7] DEVX was initially synthesized to mimic the *O*-ethyl substituent in VX, but the bulk of the diethyl phosphorus center is larger than the volume of the methyl-phosphonate moiety of VX. DMVX also contains an achiral phosphorus center, but the volume of the dimethyl center is more representative of authentic VX. The catalytic activity of the PTE variants with DMVX was surprisingly low, but this analogue captures the much lower catalytic activity of wild-type PTE for the hydrolysis of VX and the substantial increase in activity with the QF variant. The catalytic properties for the hydrolysis of DMVX are also able to predict the high k_{cat} for the hydrolysis of VX by L7ep-3a. While DEVX was intended to ensure accommodation of the larger *O*-ethyl substituent, the data for DMVX suggests that for mimicking VX, the overall size of the phosphorus center is more important. While the asymmetry of the phosphonate center is obviously a major contributor to the catalytic activity using VX as a substrate, the dimethyl center provided a reasonable prediction of the catalytic activity.

The compound DEVR was synthesized to test the significance of diethylamino vs diisopropylamino groups contained within the VR and VX leaving groups, respectively. The smaller leaving group of DEVR resulted in 2-fold less activity compared to

Table 6. Kinetic Constants for PTE Variants with V-Agent Analogues[a]

	DMVX				DEVR				OMVR[c]			
enzyme	k_{cat} (s^{-1})	K_m (mM)	k_{cat}/K_m (M^{-1} s^{-1})	fold improved	k_{cat} (s^{-1})	K_m (mM)	k_{cat}/K_m (M^{-1} s^{-1})	fold improved	k_{cat} (s^{-1})	K_m (mM)	k_{cat}/K_m (M^{-1} s^{-1})	fold improved
wild-type	0.021	1.1	1.9 × 10^1		0.201	0.38	5.6 × 10^2		nd	nd	6.8 × 10^1	
QF	0.21	0.80	2.6 × 10^2	14	0.82	0.37	2.2 × 10^3	4	0.15	1.7	7.1 × 10^1	1
CVQFL	17	3.7	4.4 × 10^3	232	1.49	0.19	7.8 × 10^3	14	nd	nd	2.1 × 10^2	3
VRN-VQFL	5.1	0.91	5.5 × 10^3	289	3.1	0.36	8.7 × 10^3	15	nd	nd	5.1 × 10^2	8
VRN-VQF-L308S[b]	3.0	1.8	1.6 × 10^3	84	1.94	0.21	9.2 × 10^3	16	nd	nd	1.4 × 10^2	2
VRN-VQFL-I106G	0.68	1.6	4.4 × 10^2	23	0.47	0.8	5.9 × 10^2	1	nd	nd	3.3 × 10^2	5
VRN-VQFL-I106G/L308S	0.3	1.15	2.6 × 10^2	14	0.115	0.97	1.2 × 10^2	0.2	nd	nd	1.9 × 10^2	3
L7ep-3a	28	2.1	1.3 × 10^4	684	6.8	0.44	1.5 × 10^4	27	1.0	1.5	5.8 × 10^2	9
L7ep-3a I106G	nd	nd	1.4 × 10^3	74	4	6	6.7 × 10^2	1	nd	nd	2.7 × 10^2	4

[a]Errors from curve fitting were less than 10% except for k_{cat} and K_m for L7ep-3aG with DEVR. [b]L308S mutation is a revertant to the wild-type amino acid sequence. [c]k_{cat}/K_m was determined from linear fit at low concentration of racemic substrate.

DOI: 10.1021/acs.biochem.5b00629
Biochemistry 2015, 54, 5502−5512

DEVX for wild-type PTE. Similar differences were obtained for most of the other variants. L7ep-3a I106G was the only variant where the catalytic activity with DEVR was less than 10% of the catalytic activity with DEVX. The relative activity between variants was similar with either leaving group but the reduced activity, especially manifested in the value of k_{cat}, suggests that the interactions of the enzyme with the leaving group may be partially responsible for aligning the phosphorus center for nucleophilic attack. The smaller leaving group probably contributes to the lower enzymatic activity observed with VR, but comparison to the catalytic activity with DEVR also highlights the dominance of the phosphorus center. The introduction of I106G in L7ep-3a resulted in a 23-fold loss of activity with DEVR, but the activity with authentic VR was improved.

In an attempt to better reflect the asymmetric phosphorus center of VR, the analogue OMVR was synthesized. The PTE variants exhibited the least activity with OMVR, which employs a slightly larger but asymmetric phosphorus center and the authentic leaving group of VR. Kinetic constants with racemic OMVR are about an order of magnitude smaller than is obtained with authentic VR, but the relative activity between variants is much more consistent than is seen with the other analogues. VRN-VQFL and L7ep-3a both have substantially better activity than wild-type PTE or QF for both OMVR and authentic VR. Introduction of I106G or removal of S308L in VRN-VQFL resulted in somewhat diminished rates for both VR and OMVR.

Active Site Hydrogen Bonding Network. The k_{cat} values for wild-type PTE with phosphorothiolate substrates are approximately 10^4-fold lower than that with the best substrates.[7,30] In the hydrolysis of substrates such as paraoxon, there is no need to protonate the leaving group.[31] In the proposed reaction mechanism for wild-type PTE, the proton from the attacking hydroxide is passed to Asp-301, and, in turn, to His-254 (Figure 4A).[24] The proton is then transferred to Asp-233 and on to bulk solvent. The variant QF has been postulated to have significantly improved catalytic activity with VX in part because of the disruption of this proton shuttle. In the crystal structure of QF, His-254 of the wild-type enzyme is a glutamine, which cannot participate in proton shuttling, and Asp-233 is moved out of hydrogen bonding distance (Figure 4B). It is thought that the "trapping" of the proton in the active site is useful for the hydrolysis of slow substrates like VX, where protonation of the leaving group will contribute to improved k_{cat} values. The crystal structure of L7ep-3a, which has a k_{cat} value for the hydrolysis of VX about an order of magnitude higher than QF, shows a remarkable rearrangement of the hydrogen bonding pattern in the active site. In L7ep-3a, Gln-254 hydrogen bonds to Asp-301, while Asp-233 has moved back into hydrogen bonding distance to Gln-254. Tyr-257 is also hydrogen bonded to Asp-301 (Figure 4C). The significant alteration of the hydrogen bonding network of Asp-301 results in the weakening of the interaction of the bridging hydroxide with the β-metal. This asymmetrical binding to the binuclear metal center is likely to result in the bridging hydroxyl being a better nucleophile. In the L7ep-3a I106G mutant, a similar hydrogen bonding pattern is observed, but Asp-233 is moved out of hydrogen bonding distance and the displacement of the bridging hydroxyl is not nearly as pronounced.

The asymmetric positioning of the bridging hydroxyl has previously been observed in the crystal structure of dihydroorotase in the presence of bound dihydroorotate.[32] Similarly, it is known that for wild-type PTE, the pK_a of the bridging water is

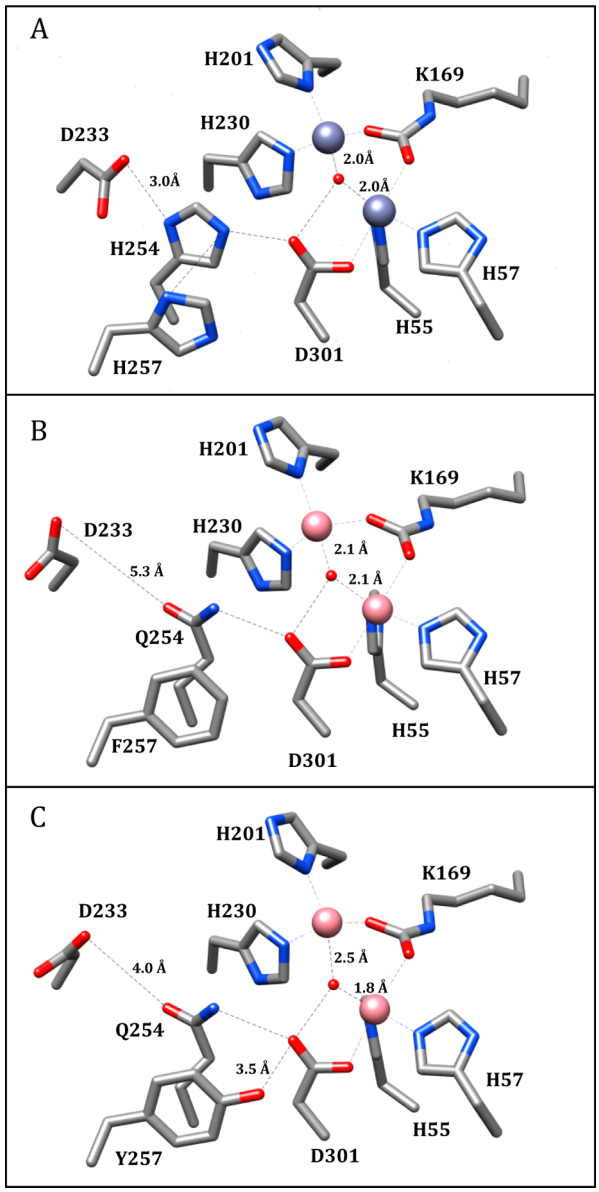

Figure 4. Metal center of wild-type PTE (A), QF (B), and L7ep-3a (C). The residues binding to the α-metal (His-55, His-57, and Asp-301), the β-metal (His-201 and His-230), and the bridging carboxylated Lys-169 are shown. The proton shuttle residues His-257, His-254, and Asp-233 are also shown. The wild-type structure is obtained from PDB id 1DPM, and the QF structure is obtained from PDB id 2OQL.

dominated by the interaction with the α-metal.[24] In wild-type PTE activated with cobalt, the pK_a determined from the pH-rate profile is 5.9 (Figure 3). The QF variant has a substantially reduced pK_a of 4.4. As has been observed with other variants, which have the putative proton shuttle disrupted, the slope of the pH-rate profile for the QF variant is +2 indicating that a second group in the active site is protonated as the pH is reduced.[24] Whether this second group is Asp-301, or possibly one of the other metal ligands, is not clear. The variant L7ep-3a, which shows asymmetric binding of the hydroxyl in the active site, exhibits the same double protonation as QF but a slightly higher pK_a of 4.6.

Docking of Substrates in the Active Site. In an effort to gain insight into the altered activity of L7ep-3a and L7ep-3a I106G, the substrates VX and VR were docked into the active site

DOI: 10.1021/acs.biochem.5b00629
Biochemistry 2015, 54, 5502−5512

using the program AutoDock Vina. Computational docking was conducted using the trigonal bipyramidal intermediates formed during the hydrolysis of both enantiomers of these compounds.[33] Productive poses were assessed by the placement of the attacking hydroxyl group between the two metal ions and the orientation of the phosphoryl oxygen toward the β-metal.[34] For the wild-type PTE and QF, both enantiomers of VX and VR could be reasonably docked into the active site (data not shown). However, for L7ep-3a and L7ep-3a I106G, only the S_P-enantiomer of VR could be reasonably positioned in the active site. For both of these variants, the constriction of the active site appears to play an important role in the improved activity, while specific mutations accommodate the substrates (Figure 5). The

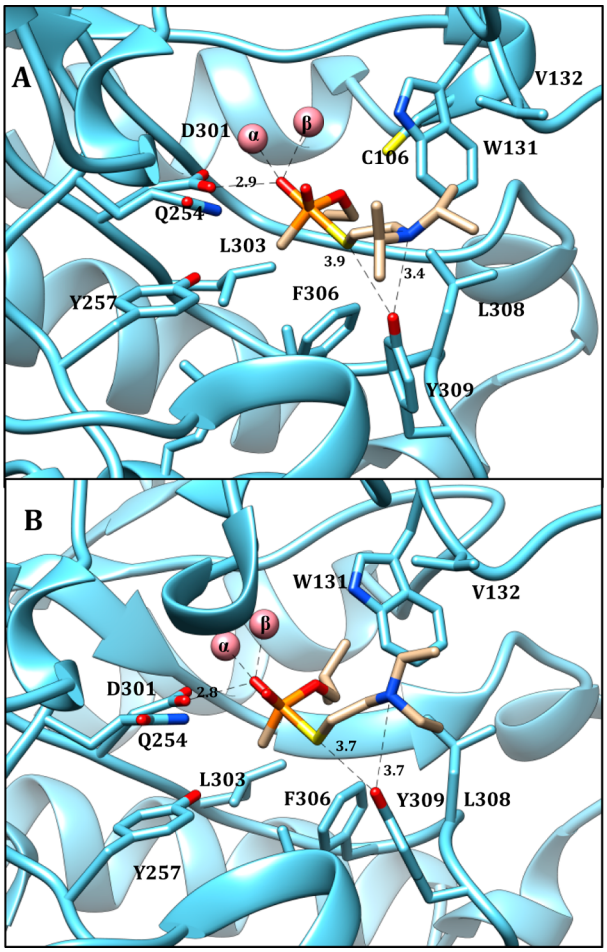

Figure 5. (A) S_P-VX docked in the active site of L7ep-3a. (B) S_P-VR docked into the active site of L7ep-3a I106G. The substrate binding residues are shown. The distances from Tyr-309 and Asp-301 are shown in units of ångstroms.

mutation F132V provides the extra room to accommodate the isopropyl amino group of VX. This effect is not as obvious with the smaller substituent contained within the leaving group in VR. The additional space in the small-group pocket due to the I106G mutation accommodates the isobutyl group in S_P-VR, while the combination of the H257Y mutation and repositioning of Tyr-309 make binding of the R_P-enantiomer more difficult. The changes in the active site also enable the sulfur and the nitrogen of the leaving group to potentially hydrogen bond with the side chain phenol of Tyr-309, suggesting that this interaction may be partially responsible for the dramatically improved activity. Tyr-309 was previously ruled out as playing a role in substrate activation with paraoxon.[24] The L7ep-3a-Y309F mutant shows kinetics virtually identical to L7ep-3a for the hydrolysis of paraoxon, but with DEVX as the substrate k_{cat}/K_m is reduced nearly 3-fold for the L7ep-3a-Y309F variant, demonstrating that the interaction of the phenolic oxygen with the leaving group is helpful for hydrolysis of the V-agents.

The determination of the three-dimensional structure of L7ep-3a has led to a greater understanding of the underlying mechanisms by which the hydrolysis of V-agents is enhanced. The determination of this structure has guided the rational construction of the new L7ep-3a I106G mutant, which VR and chiral center analogue data suggest is enhanced 620-fold for the hydrolysis of the S_P-enantiomer of VR, relative to the wild-type enzyme. Previous work with the insecticide demeton-S demonstrated the importance of the leaving group on the catalytic activity of PTE, and our results with the new analogues of VR and VX has further demonstrated that even small changes in the leaving group can have dramatic effects on the activity of the enzyme.[7] The crystal structures of L7ep-3a and L7ep-3a I106G have provided a physical basis for these observations. The computational docking results have suggested how the remodeled active site is able to exploit hydrogen bonding interactions with Tyr-309. The disruption of the proton shuttle, along with new hydrogen bonds to Asp-301, are apparently able to enhance the attack of the bridging hydroxide on phosphorothiolate substrates. The initial data with the new racemic analogue OMVR suggests that the combination of an asymmetric phosphorus center and the authentic leaving group of VR will allow for much more accurate predictions of the activity against VR and enable the more rapid development of new variants that are more fully optimized for the hydrolysis of VR.

AUTHOR INFORMATION

Corresponding Author

*Telephone: 979-845-3373. Fax: 979-845-9452. E-mail: raushel@tamu.edu.

Funding

This work was supported by the Defense Threat Reduction Agency (HDTRA1-14-1-0004).

Notes

The authors declare no competing financial interest.

ACKNOWLEDGMENTS

We are grateful to the laboratory of Professor James C. Sacchettini for assistance in collecting the X-ray crystallographic data.

ABBREVIATIONS

PTE, phosphotriesterase; DEVX, *O*,*O*-diethyl VX; DMVX, *O*,*O*-dimethyl VX; DEVR, *O*,*O*-diethyl VR; OMVR, *O*-methyl VR; APVR, *p*-acetophenyl VR; VX, *S*-(2-(diisopropylamino)ethyl) *O*-ethyl methylphosphonothioate; VR, *S*-(2-(diethylamino)-ethyl) *O*-isobutyl methylphosphonothioate; PON1, paraoxonase I from humans; DFPase, diisopropylfluorophosphatase from *Loligo vulgaris*; OPAA, organophosphorus acid anhydrolase from *Alteromonas* sp; DTNB, 5,5′-dithiobis(2-nitrobenzoic acid)

DOI: 10.1021/acs.biochem.5b00629
Biochemistry 2015, 54, 5502−5512

REFERENCES

(1) Benschop, H. P., and De Jong, L. P. A. (1988) Nerve agent stereoisomers: analysis, isolation and toxicology. *Acc. Chem. Res. 21*, 368−374.

(2) Rosman, Y., Eisenkraft, A., Milk, N., Shiyovich, A., Ophir, N., Shrot, S., Kreiss, Y., and Kassirer, M. (2014) Lessons Learned From the Syrian Sarin Attack: Evaluation of a Clinical Syndrome Through Social MediaLessons Learned From the Syrian Sarin Attack. *Ann. Intern. Med. 160*, 644−648.

(3) Leikin, J. B., Thomas, R. G., Walter, F. G., Klein, R., and Meislin, H. W. (2002) A review of nerve agent exposure for the critical care physician. *Crit. Care Med. 30*, 2346−2354.

(4) Columbus, I., Waysbort, D., Marcovitch, I., Yehezkel, L., and Mizrahi, D. M. (2012) VX Fate on Common Matrices: Evaporation versus Degradation. *Environ. Sci. Technol. 46*, 3921−3927.

(5) Saxena, A., Sun, W., Fedorko, J. M., Koplovitz, I., and Doctor, B. P. (2011) Prophylaxis with human serum butyrylcholinesterase protects guinea pigs exposed to multiple lethal doses of soman or VX. *Biochem. Pharmacol. 81*, 164−169.

(6) FLIR Systems Threat Detection Technologies: Enzymes, FLIR Systems, Wilsonville, OR, http://www.flir.com/threatdetection/display/?id=63297 (accessed 8/4/15).

(7) Bigley, A. N., Xu, C., Henderson, T. J., Harvey, S. P., and Raushel, F. M. (2013) Enzymatic neutralization of the chemical warfare agent VX: evolution of phosphotriesterase for phosphorothiolate hydrolysis. *J. Am. Chem. Soc. 135*, 10426−10432.

(8) Cheng, T., Liu, L., Wang, B., Wu, J., DeFrank, J. J., Anderson, D. M., Rastogi, V. K., and Hamilton, A. B. (1997) Nucleotide sequence of a gene encoding an organophosphorus nerve agent degrading enzyme from Alteromonas haloplanktis. *J. Ind. Microbiol. Biotechnol. 18*, 49−55.

(9) Gupta, R. D., Goldsmith, M., Ashani, Y., Simo, Y., Mullokandov, G., Bar, H., Ben-David, M., Leader, H., Margalit, R., Silman, I., Sussman, J. L., and Tawfik, D. S. (2011) Directed evolution of hydrolases for prevention of G-type nerve agent intoxication. *Nat. Chem. Biol. 7*, 120−125.

(10) Kirby, S. D., Norris, J. R., Richard Smith, J., Bahnson, B. J., and Cerasoli, D. M. (2013) Human paraoxonase double mutants hydrolyze V and G class organophosphorus nerve agents. *Chem.-Biol. Interact. 203*, 181−185.

(11) Melzer, M., Chen, J. C., Heidenreich, A., Gab, J., Koller, M., Kehe, K., and Blum, M. M. (2009) Reversed enantioselectivity of diisopropyl fluorophosphatase against organophosphorus nerve agents by rational design. *J. Am. Chem. Soc. 131*, 17226−17232.

(12) Tsai, P. C., Fox, N., Bigley, A. N., Harvey, S. P., Barondeau, D. P., and Raushel, F. M. (2012) Enzymes for the homeland defense: optimizing phosphotriesterase for the hydrolysis of organophosphate nerve agents. *Biochemistry 51*, 6463−6475.

(13) Oudejans, L. (2013) *Evaluation Report EPA 600/R-12/033: Enzymatic Decontamination of Chemical Warfare Agents*, United States Envirnmental Protection Agency, Washinton D.C.

(14) Scott, C. (2012) *Landguard A900: An enzyme-based remdiant for the detoxification of organophosphate insecticides in animal dips*, CSIRO Ecosystem Science, Canberra, Australia, https://publications.csiro.au/rpr/download?pid=csiro:EP125235&dsid=DS2 (accessed 8/4/15).

(15) LeJeune, K. E., and Russell, A. J. (1999) Biocatalytic nerve agent detoxification in fire fighting foams. *Biotechnol. Bioeng. 62*, 659−665.

(16) Tsai, P. C., Bigley, A., Li, Y., Ghanem, E., Cadieux, C. L., Kasten, S. A., Reeves, T. E., Cerasoli, D. M., and Raushel, F. M. (2010) Stereoselective hydrolysis of organophosphate nerve agents by the bacterial phosphotriesterase. *Biochemistry 49*, 7978−7987.

(17) Mee-Hie Cho, C., Mulchandani, A., and Chen, W. (2006) Functional analysis of organophosphorus hydrolase variants with high degradation activity towards organophosphate pesticides. *Protein Eng., Des. Sel. 19*, 99−105.

(18) Roodveldt, C., and Tawfik, D. S. (2005) Directed evolution of phosphotriesterase from Pseudomonas diminuta for heterologous expression in Escherichia coli results in stabilization of the metal-free state. *Protein Eng., Des. Sel. 18*, 51−58.

(19) Rastogi, V. K., DeFrank, J. J., Cheng, T. C., and Wild, J. R. (1997) Enzymatic hydrolysis of Russian-VX by organophosphorus hydrolase. *Biochem. Biophys. Res. Commun. 241*, 294−296.

(20) Cherny, I., Greisen, P., Jr., Ashani, Y., Khare, S. D., Oberdorfer, G., Leader, H., Baker, D., and Tawfik, D. S. (2013) Engineering V-type nerve agents detoxifying enzymes using computationally focused libraries. *ACS Chem. Biol. 8*, 2394−2403.

(21) Reiter, G., Muller, S., Hill, I., Weatherby, K., Thiermann, H., Worek, F., and Mikler, J. (2015) In vitro and in vivo toxicological studies of V nerve agents: molecular and stereoselective aspects. *Toxicol. Lett. 232*, 438−448.

(22) Amitai, G., Ashani, Y., Grunfeld, Y., Kalir, A., and Cohen, S. (1976) Synthesis and properties of 2-S-(N,N-dialkylamino)ethyl)thio-1,3,2-dioxaphosphorinane 2-oxide and of the corresponding quaternary derivatives as potential nontoxic antiglaucoma agents. *J. Med. Chem. 19*, 810−813.

(23) Michaelis, L., and Menten, M. L. (1913) Die Kinetik der Invertinwirkung. *Biochem. Z. 49*, 333−369.

(24) Aubert, S. D., Li, Y., and Raushel, F. M. (2004) Mechanism for the hydrolysis of organophosphates by the bacterial phosphotriesterase. *Biochemistry 43*, 5707−5715.

(25) Otwinowski Z, M. W. (1997) Processing of X-ray diffraction data collected in oscillation mode. *Methods Enzymol. 276A*, 307−326.

(26) Adams, P. D., Afonine, P. V., Bunkoczi, G., Chen, V. B., Davis, I. W., Echols, N., Headd, J. J., Hung, L.-W., Kapral, G. J., Grosse-Kunstleve, R. W., McCoy, A. J., Moriarty, N. W., Oeffner, R., Read, R. J., Richardson, D. C., Richardson, J. S., Terwilliger, T. C., and Zwart, P. H. (2010) PHENIX: a comprehensive Python-based system for macromolecular structure solution. *Acta Crystallogr., Sect. D: Biol. Crystallogr. 66*, 213−221.

(27) Emsley, P., and Cowtan, K. (2004) Coot: model-building tools for molecular graphics. *Acta Crystallogr., Sect. D: Biol. Crystallogr. 60*, 2126−2132.

(28) Trott, O., and Olson, A. J. (2010) AutoDock Vina: Improving the speed and accuracy of docking with a new scoring function, efficient optimization, and multithreading. *J. Comput. Chem. 31*, 455−461.

(29) Chen-Goodspeed, M., Sogorb, M. A., Wu, F., Hong, S. B., and Raushel, F. M. (2001) Structural determinants of the substrate and stereochemical specificity of phosphotriesterase. *Biochemistry 40*, 1325−1331.

(30) Caldwell, S. R., Newcomb, J. R., Schlecht, K. A., and Raushel, F. M. (1991) Limits of diffusion in the hydrolysis of substrates by the phosphotriesterase from Pseudomonas diminuta. *Biochemistry 30*, 7438−7444.

(31) Hong, S. B., and Raushel, F. M. (1996) Metal-substrate interactions facilitate the catalytic activity of the bacterial phosphotriesterase. *Biochemistry 35*, 10904−10912.

(32) Thoden, J. B., Phillips, G. N., Neal, T. M., Raushel, F. M., and Holden, H. M. (2001) Molecular Structure of Dihydroorotase: A Paradigm for Catalysis through the Use of a Binuclear Metal Center. *Biochemistry 40*, 6989−6997.

(33) Caldwell, S. R., Raushel, F. M., Weiss, P. M., and Cleland, W. W. (1991) Transition-state structures for enzymatic and alkaline phosphotriester hydrolysis. *Biochemistry 30*, 7444−7450.

(34) Vanhooke, J. L., Benning, M. M., Raushel, F. M., and Holden, H. M. (1996) Three-Dimensional Structure of the Zinc-Containing Phosphotriesterase with the Bound Substrate Analog Diethyl 4-Methylbenzylphosphonate. *Biochemistry 35*, 6020−6025.

DOI: 10.1021/acs.biochem.5b00629
Biochemistry 2015, 54, 5502−5512